2-2021

Fabrication Of Nanocrystalline Austenitic Stainless Steel with Superior Strength and Ductility Via Binder Assisted Extrusion Method

L. Heidari
Shiraz University

M. J. Hadianfard
Shiraz University

A. R. Khalifeh
Shiraz Petrochemical Complex

Daryoosh Vashaee
North Carolina State University

Lobat Tayebi
Marquette University, lobat.tayebi@marquette.edu

Powder Technology, Vol. 379 (February 2021): 38-48. DOI.

Fabrication Of Nanocrystalline Austenitic Stainless Steel with Superior Strength and Ductility Via Binder Assisted Extrusion Method

L. Heidari
Department of Materials Science and Engineering, School of Engineering, Shiraz University, 71348-51154 Shiraz, Iran
M.J. Hadianfard
Department of Materials Science and Engineering, School of Engineering, Shiraz University, 71348-51154 Shiraz, Iran
A.R. Khalifeh
Inspection and Corrosion Prevention Department, Shiraz Petrochemical Complex, Shiraz, Iran
D. Vashaee
Electrical and Computer Engineering Department, North Carolina State University, Raleigh, NC
L. Tayebi
Marquette University School of Dentistry, Milwaukee, WI

Abstract

Biomedical austenitic stainless steel (ASTM F2581) has been processed by the powder metallurgy technology using binder assisted extrusion method and aside a sintering aid. The resultant microstructure was examined by optical microscopy, field emission scanning electron microscopy, transmission electron microscopy and x-ray diffraction methods. The optical microscopy images indicate that using the binder and sintering aid considerably decreases the porosities of the sintered samples. The x-ray diffraction and transmission electron microscopy images reveal that the microstructure of the sintered alloy consists of austenite in nanocrystalline form and amorphous phases. The mechanical properties were measured through compressive tests. The mean yield strength is estimated at about 824 MPa, and the compressive strength exceeds 1GPa, which is superior to the austenitic stainless steel produced through the conventional methods. Furthermore, the process followed here is compatible with large scale industrial production at a reasonable cost.

Graphical abstract

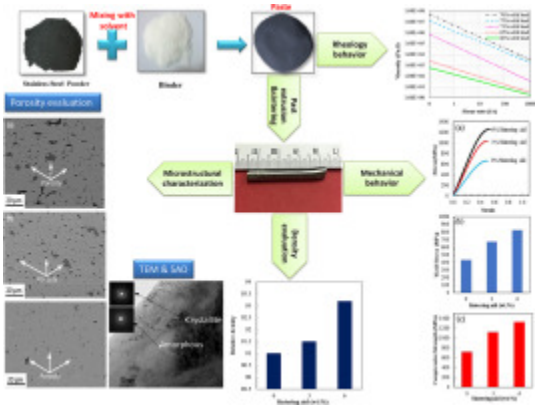

Keywords

Medical grade stainless steel, Binder assisted extrusion method, Nanostructure

1. Introduction

Austenitic stainless steels are used in medical applications, such as implants and orthodontic devices, extensively [[1], [2], [3]]. However, many problems have been reported with using this group of materials in human bodies. The most significant problem issue is associated with the metal ions or fretting debris—such as nickel ion—being freed from the implants in the organs due to the corrosion and wear phenomenon. The released nickel ions act as allergens in the human body, which can cause inflammation, like itching and swelling of skin [[4], [5], [6]]. Due to the negative impacts of nickel ions on body tissues, nickel-free austenitic stainless steel systems, like Fe–Cr–Mn–Mo–N, have been advised as a replacement for typical nickel-containing alloys [7,8]. Nickel is an austenite stabilizer in austenitic stainless steels or 18–8 stainless steel groups. In the nickel-free steel grades, nitrogen is used instead of nickel to stabilize the austenite phase [9].

Several methods—including powder metallurgy, melting processes and solid nitrogen absorption treatment—have been developed to produce nitrogen containing nickel-free austenitic stainless steels. Powder metallurgy is a unique technique in which metallic and alloy materials are produced from the

metal powders in a wide variety of shapes and applications [10]. The high precision forming potential of powder metallurgy creates components with a final shape and complex structure, without the need to use metal removal processes such as machining [11]. In the powder metallurgy method, the powder of nickel-free stainless steel is mostly prepared using the mechanical alloying technique. The mechanical alloying is the process of synthesizing a wide variety of microstructures, including the supersaturated, metastable crystallite and nanostructured ones [11]. Nanostructured metallic materials with the nanocrystalline and ultrafine-grained structure show special mechanical properties, e.g., superior yield stress, strength and hardness [[12], [13], [14], [15]]. The yield stress, ultimate strength and hardness are increased due to decreasing the grain size, reaching ultra-high values at very small grain sizes, mainly due to the blocking of dislocations from slipping by grain boundaries [[16], [17], [18], [19]]. Increasing the strength leads to a reduction in the dimensions of components and their weights [20], which appeals to its use in medical applications.

There are several ways to process the milled powders and manufacture the steel parts with the powder metallurgy including hot extrusion, hot forging, hot isostatic pressing (HIP), metal injection molding (MIM), press sintering (PS), and so forth [[21], [22], [23]]. Most of these methods require a combination of high temperature with high pressure for fabricating a component, making it complicated and expensive to proceed. Additionally, in some methods such as HIP, it is not possible to build large components [24]. The PS method has been used for the fabrication of nickel-free stainless steels (ASTM F2581) in our laboratory [25]. Limitations and disadvantages of the PS—such as difficulties in achieving a high density, a challenge in fabricating large size parts, and high cost of the processing method—provide the primary motivation for investigation of new techniques with more capabilities. To solve these problems, we consider the binder assisted extrusion method (BAE) in this investigation for the processing of the alloy. This method is another powder metallurgy process in which a binder facilitates the formability of the powders and makes it possible to produce the large samples [24,26].

The BAE method is a unique process for fabricating ceramic components [27]. In the manufacturing of the ceramic parts by powder technology, the powders are often non-plastic and require the use of some additives for improving their formability [28]. Research has demonstrated utilizing binders that mix well with ceramic powders provides a paste with adequate rheological characteristics, improving their formability during extrusion processes. These binders also stabilize the shapes of extruded parts after the extrusion operation [[29], [30], [31], [32], [33]].

Based on this concept in this study, a polymeric binder is utilized for the first time in the production processes of the nickel-free austenitic stainless steel (ASTM F2581 grade). A sintering aid component (Mn-11.5 wt% Si) with 0, 3 and 6 wt% is also added to improve the sintering treatment and facilitate the manufacturing process. The processing treatment of the green sample is completed at ambient temperature without using a high pressure. For this reason, it is not necessary to use a high temperature mold and an expensive hot press system in the forming process. The high temperature mold requires a heating system that increases the cost of production. On the other hand, the depreciation of the high temperature mold is much higher than low temperature mold, and thus, the cost of renovating the mold should be considered.

Significant microstructural and mechanical properties are also achieved using the binder aside from the sintering aid. Significantly, the binder makes it possible to produce large and flawless components. It should be noted that the corrosion resistance and biocompatibility behavior of ASTM F2581 proceed via the PS method were investigated by our group [34]. The results reveal that the alloy has proper biocompatibility behavior and, therefore, this paper does not provide further information regarding this topic.

2. Material and methods

The primary aim of this investigation is to fabricate the nickel-free stainless steel ASTM F2581 using the BAE powder metallurgy technique. The summary of the process is schematically shown in Fig. 1.

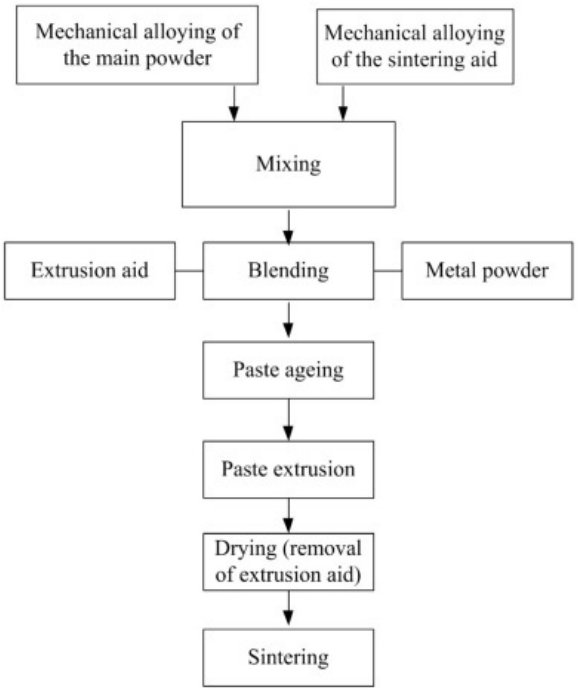

Fig. 1. The synthesis steps for the production of Ni-free stainless steel.

2.1. Powder preparation

Atomic elements of iron, chromium, molybdenum, manganese and silicon supplied by Merck and Fe_3N as a supplier of nitrogen alloy were mixed and ball milled with a ball to powder weight ratio of 20:1 under the protection of argon atmosphere. The nickel-free stainless steel powders were developed after 48 h milling. Sintering aid powders (Mn–11.5 wt% Si) have been prepared in the same way and were added by 0, 3 and 6 wt% to the stainless steel powders. The composition of the fabricated alloy powders is Fe-17Cr-10Mn-3Mo-0.4Si-0.5 N-0.2C wt% (ASTM F2581), with an average particle size of 10 μm. The detail of the powder fabrication is presented elsewhere [10]. The shape and size of the alloy and sintering aid (Mn-11.5 wt% Si) powders are shown in Fig. 2.

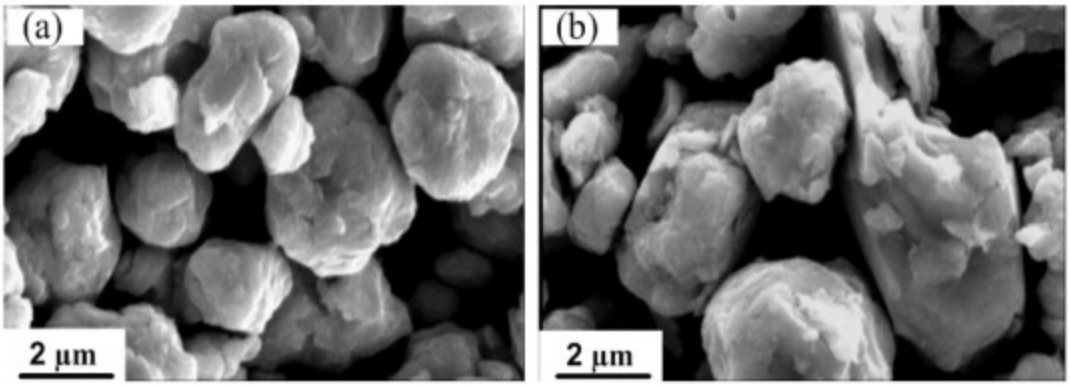

Fig. 2. SEM image of the milled (a) ASTM F2581 and (b) sintering aid powders.

2.2. Paste preparation

The paste preparation was completed by mixing the alloy powder and binder, resulting in the high viscose fluid. The binder is a mixture of several polymers that reduces friction between the solid particles and facilitates the movement of powder particles for more proper shaping treatment. The binder consists of 20 wt% adhesive, 30 wt% plasticizer, 5 wt% dispersant and 45 wt% solvent. The optimum amounts of the components in the binder have been determined from the Taguchi model. For the paste preparation, polyvinyl pyrrolidone (PVP), ethylene glycol and stearic acids are used as an adhesive, plasticizer and dispersant, respectively, with cyclohexane utilized as a solvent. The solid powders consist of ASTM F2581 alloy and Mn-11.5 wt% Si sintering aid. The solid powder of ASTM F2581 containing 0, 3 and 6 wt% sintering aid were prepared according to Javanbakht recommendation [35]. The solvent, adhesive and plasticizer were well mixed in a shear mixing system at 100 rpm. To obtain a uniform paste, the adhesive and plasticizer were dissolved in the cyclohexane solvent, and then the alloy powder was added and mixed in the shear mixing system. In the next step, the solvent was added to the mixture slowly until a uniform paste with good formability was obtained. The paste was stored for about 4 h in a nylon protector for the volatilization of the solvent and aging process.

2.3. Quality control of the paste

The rheological behavior of the paste with 60, 65, 70, 71, 75 and 76 vol% of solid powders was investigated by a torque rheometry test through measuring the viscosity versus shear rate. These concentrations are selected based on the work of other investigators [36]. The solid powders in this test consist of 94 wt% ASTM F2581 alloy and 6 wt% sintering aid. A capillary rheometer (RH 2200 Rosand,) was used for this measurement.

2.4. Paste extrusion and sintering

The prepared pastes were extruded at a pressure of 5 MPa through a floating die in a conventional rod extrusion method. A die with a hole diameter of 4 mm, semi-angle of 90° (flat die) and die land length of 10 mm was used with an extrusion ratio of 10. The extrusion treatment was carried out at a constant speed of 1 mm/s at room temperature. The use of polymer facilitated the initial forming processes at room temperature. As mentioned earlier, the current technique has been used to make ceramic parts. One of the important advantages of this method is its cost effectiveness and accessibility of the required equipment. A simple press and an ordinary furnace are the only

instruments needed to fabricate the part with this method. The alloy was produced using the hot powder forging technique in our laboratory [36]. Moreover, the issue of limitation of large sample parts production by the hot powder forge was resolved in the BAE method. In the next step, the extruded sample that contained the binder (known as the green sample) was placed at a temperature of 550 °C at a neutral atmosphere to remove the binder. The sample, after removing the binder, is called the brown sample. The brown sample was then encapsulated in an evacuated quartz crystal and sintered for 60 min at a temperature of 1150 °C. This sintering temperature is the optimum temperature for sintering the alloy, stated by Javanbakht during PS method processing [10]. Finally, the sample was immediately cooled in water to maintain the high-temperature austenitic structure at room temperature [37]. A typical material produced by this method is presented in Fig. 3.

Fig. 3. Typical of ASTM F2581 alloy produced utilizing the BAE method.

2.5. Specimen characterization

Microstructural characterization of the green, brown and sintered samples was conducted by scanning electron microscopy (SEM) and field emission electron microscopy (FE-SEM). The microstructures of the sintered samples were also studied by optical microscopy after polishing and etching by the oxalic acid etchant. The x-ray diffraction technique was used to analyze phase formation and measure crystallite sizes after sintering. The quantitative analysis of XRD data was completed using Maoud software [35]. The relative content of present phases and crystallite size were estimated by the Rietveld analysis. The amorphous phase content was also determined by the Rietveld analysis of the XRD patterns. The known amount of nanocrystalline Fe powder was used as a standard, as detailed in Ref. [14].

The validity of the XRD results was verified by transmission electron microscopy (TEM). To prepare the TEM sample, a sintered specimen was cut into a disk of 3 mm in diameter, ground to approximately 100 µm in thickness, then electropolished to obtain a few micrometer thickness specimens. The porosity level and density of the samples are two critical parameters that significantly affect their properties. Therefore, the size, shape and percentage of porosities of the sintered specimens were investigated by optical microscopy (OM), scanning electron microscopy (SEM) and image analyzer software. The density of the samples was measured by the Archimedes method.

2.6. Mechanical testing

The microhardness properties of sintered samples were obtained by the Vickers method. At least five randomly-located points were measured to obtain the hardness of samples, and then the average values were reported. The compression strength of the prepared samples was measured using the

uniaxial compressive tests, according to ASTM:E9 [38]. The cylindrical samples with an aspect ratio of 1.5 were used. The compression tests were done at a constant speed of 0.1 mm/s, with at least three replicates to ensure the results. Testing continued up to 50% deformation for all samples. The results have been obtained in terms of Force-Displacement, and then converted to the engineering stress-strain data.

3. Results and discussion

3.1. Paste fabrication

The initial stage of the manufacturing process is the paste preparation. The rheology behavior of the paste has a strong influence on the quality of the production piece. The interesting point of this research is the use of a set of polymers as a binder in the paste to facilitate the extrusion process at room temperature. The paste properties are strongly dependent on the amount of the alloy powder and binder in the mixture. In particular, the formability of the paste is an essential characteristic in the forming process, which is strongly influenced by the viscosity. The low amount of polymer increases the viscosity and reduces the formability of the paste, which may create a cavity in the molding processes. High polymer content is also not appropriate, as it may cause solid particles to separate and paste to behave similar to a fluid [39].

Luoe et al. [40] developed an equation that expresses the relationship between viscosity and load change rate in back extrusion experiment as:

(1)

$$\eta_{app} = \frac{1}{2\pi\lambda C V_p} . \frac{dF}{dt}$$

where η_{app} is the viscosity, V_p is the punch velocity, λ is the extrusion ratio, *dF/dt* is the load change rate and C is a constant. According to Eq. (1), a decrease in viscosity decreases the load change rate. This indicates that when the viscosity is low, the paste is easily extruded or shows proper formability. On the other hand, the viscosity is affected by the solid powder ratio. The ratio of the solid powder to solid powder plus binder is expressed as follows:

(2)

$$\varphi = \frac{W_p/\rho_p}{W_p/\rho_p + W_b/\rho_b} . 100$$

where φ is solid load, and W_p and W_b are weight of the alloy powder and the binder (polymer), respectively. Meanwhile, ρ_p and ρ_b are the powder and the binder densities, respectively [39].

Generally, the solid powders for a paste should contain more than 60% solid load [41]. To determine the optimum condition, we start from this ratio and 5% lower. Therefore, the pastes with 55, 60, 65, 71, 75 and 76 vol% solid loads were fabricated. The viscosity variations of prepared pastes with shear rate were examined using a rheometer. The change in log-log presentation of viscosity versus shear rate is shown in Fig. 4. The solid powder here contains 6 wt% sintering aid. The results clearly show a reduction in the viscosity of the paste with an increase in the shear rate. This phenomenon is known as

shear-thinning. Shear thinning occurs due to the breakdown of the floccule particles, which prevents the paste from flocculation. Our paste demonstrates non-Newtonian pseudoplastic behavior [42]. The same trend has been observed for the samples containing 0 and 3 wt% sintering aid.

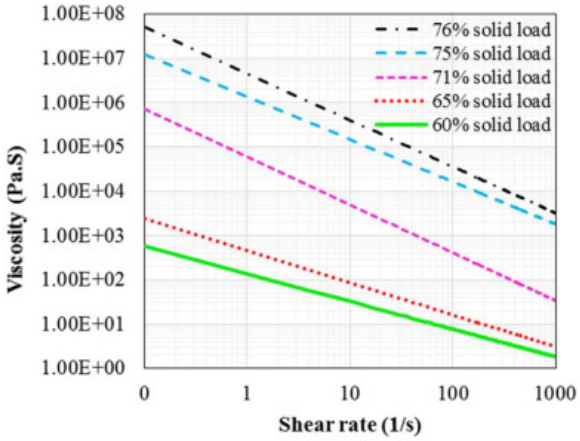

Fig. 4. The variation of the viscosity with shear rate for 60, 65, 71, 75 and 76 vol% solid load in 6 wt% sintering aid.

The mixer available in our laboratory works at a shear rate of 30 s^{-1}. Therefore, the viscosity data of this shear rate versus solid load is taken from Fig. 4 and is plotted in Fig. 5. Also, the effects of adding 0, 3 and 6 wt% sintering aid on the viscosity were investigated in this stage (Fig. 5). In general, the viscosities tend to increase with increasing the solid load. Fig. 5 shows that this trend for metals powder containing 0, 3 and 6 wt% sintering aid is about the same. The results also indicate that an increase in sintering aid value causes a small decrease in the viscosity for all ranges of the solid powders.

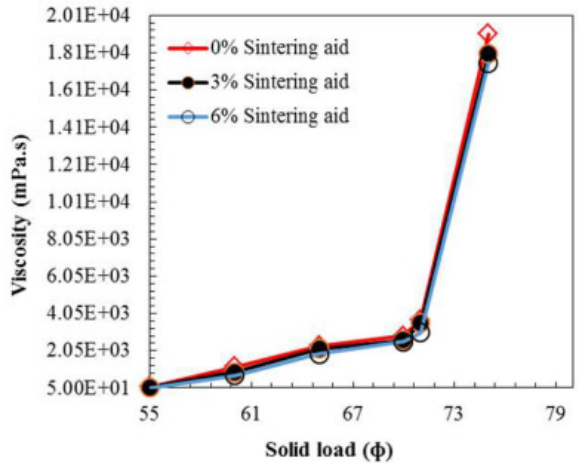

Fig. 5. The viscosity changes in terms of solid-phase percent at a shear rate of 30 S^{-1} for 0, 3 and 6 wt% sintering aid.

There are many factors, including the hardness, shape and size of solid particles that affect the viscosity properties of pasts [26]. The shape and size of particles for the metal and sintering aid that have been used in the present study are almost similar (Fig. 2). Therefore, these factors do not cause a significant change in viscosity behavior of the paste. The sintering aid (Mn–11.5 wt% Si) has less

strength than ASTM F2581, so less friction is creating with adding sintering aid in solid powder. This results in a slight decrease in the viscosity of the paste, as seen in Fig. 4.

With attention to Fig. 5, it can be seen that a small increase in the viscosity of the mixture with an increase in the solid load amount up to the value of φ equal to 71 vol%. At this point, a sharp rise in the viscosity is revealed. The polymer creates a lubricating property between the particles. In this ratio of solid load and higher, the amount of polymer is low, and the lubrication between the particles is not enough, so the viscosity rise up. The viscosity has an inverse relationship with the paste formability [43]. This means that as viscosity increases, the paste formability decreases, and processes are not economical. Therefore, for the paste preparation, the percentage of the solid load in the mixture should not be more than this ratio. The graph shows that the viscosity is small when the parameter is under 55 vol%. In other words, the mixture shows very low viscosity and very high formability with solid load lower than 55 vol%, but the problem in this area is that the paste is not stable and appears to be a fluid. This instability has occurred because the binder value is higher than the amount required for powder wetting. So, a ratio of less than 55 vol% is rejected. The same test has been completed on the sample with a 60 vol% solid load. The results reveal that for this sample, the viscosity is low enough and formability is excellent. Therefore, according to the results of the rheometry, the solid load portion should be in the range of 60–71 vol%. Chen et al. has completed investigations on the behavior of stainless steel pastes, and recognized that this range of solid loads provide suitable viscosity [26].

Another critical factor in the paste preparation process is the cold extrusion capability. Fig. 6 shows the typical extrusion pressure versus extrusion stroke for samples with 60, 65 and 71 vol% solid loads. As seen for the sample with φ equal to 71 vol%, the extrusion pressure increases in the initial stage and then remains constant up to a distance where a sharp increase occurs. A phenomenon that occurs at ϕ equal 71 vol% and above is the separation of the binder from the paste. Because of this, the lubricant processes are not sufficient and cause an increase in the internal friction between the powders. This leads to the increase in the pressure required for incremental of densification as compaction progresses. This area is known as the dead zone.

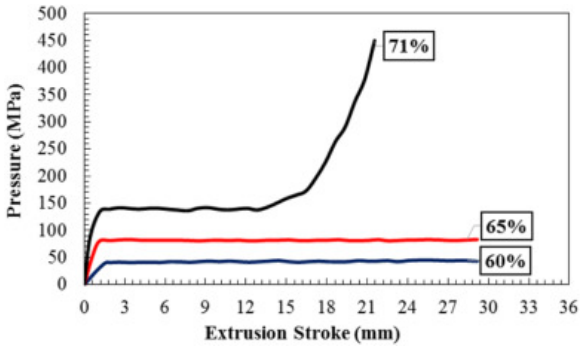

Fig. 6. Extrusion pressure vs. stroke curves obtained from forming of the stainless steel pastes by rod extrusion method in 60, 65 and 71 vol% solid load.

In the case of φ equal 60%, the initial increase in the extrusion pressure is seen, which is followed by constant pressure. No growth is found for this solid load; however, instability of the extruded paste is deemed problematic. The stability of extruded paste depends on the values of the binder between the particles. The presence of high amount of binders in this sample causes the particles to slip with low

force, and the instability of the formed part occurs [43]. For the paste sample with ϕ equal 65%, the initial increase in the extrusion pressure is also seen, which continues in a constant pressure region. No substantial increase in extrusion pressures at the end of extrusion stroke is observed, and the shape of the final pieces is also adequately stable. In addition, the sample with 65 wt% solid load contained fewer defects and had higher density. Therefore, this solid load is selected as the optimal condition for the paste preparation.

The SEM images of the green, brown and sintered samples containing 6 wt% sintering aid are shown in Fig. 7. Fig. 7a is the image of the green sample and a thin layer of the binder—which covers all particles—can be seen in the picture. To show the presence of polymer in the green sample, BSE (Back Scatter Electron) technique and EDS analysis was utilized. A thin layer of polymer is marked on the BSE image of the green sample (Fig. 7a). The EDS analysis reveals a sharp peak for carbon on this sample. The polymers mostly consist of C and H elements. The appearance of sharp carbon peak for this sample proves the presence of polymer on the particles.

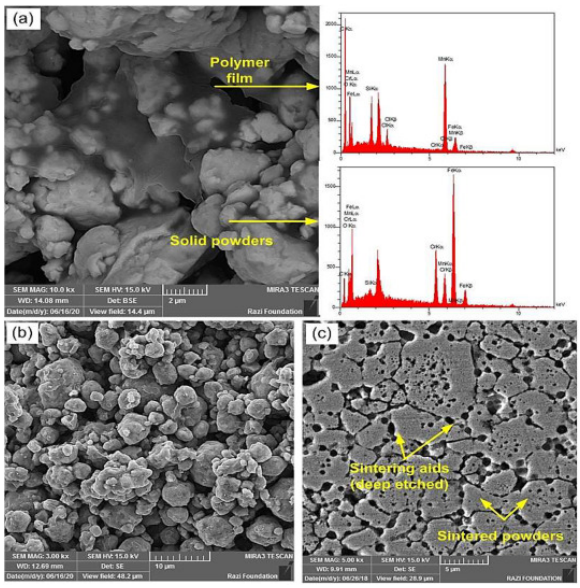

Fig. 7. SEM images of (a) green sample, (b) brown sample and (c) FE-SEM image of the sintered sample. (For interpretation of the references to colour in this figure legend, the reader is referred to the web version of this article.)

Fig. 7b shows the micrograph image of the brown sample. The image indicates that the binder has entirely left the sample, and bridges between the powders have been appropriately created. This is an initial stage of the sintering processes [44]. Fig. 7c displays the FE-SEM photograph of the sintered sample after the chemical etching. As seen, the connection between the powder particles has been established entirely during the sintering processes. Fig. 8 presents an image of the sample containing 6 wt% sintering aid that was polished and etched by oxalic acid solution. The austenite and some porosity are visible in the microstructure. Some of the porosities seen in the sintered powder boundaries are related to the sintering aids. The EDS analysis has been obtained from this area. The result is presented on the right side of Fig. 8 and confirms presence of sintering aid in the microstructure.

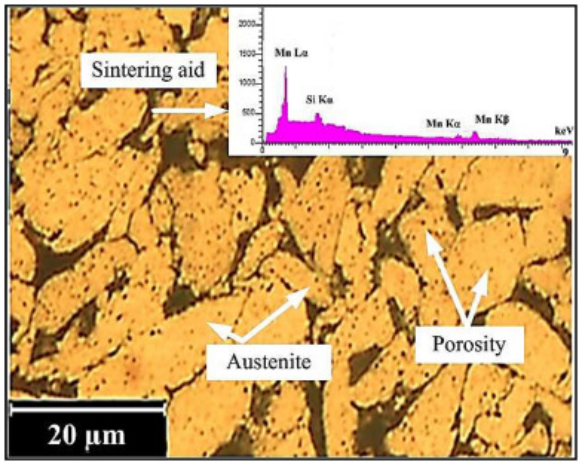

Fig. 8. Optical micrograph of the etched and polished sample contain 6 wt% sintering aid sintered at 1150 °C.

ASTM F2581 is a corrosion resistant alloy that exhibits exceptional resistance to corrosive environments Meanwhile, the Mn—Si additive is a common alloy that shows low resistance to the corroded solution and appear as pores in the etched microstructure [44]. The corrosion resistance of ASTM F2581 is due to formation of the spontaneously formed passive films on its surface in aqueous solutions or under the influence of moist air [45]. Moreover, Gavriljuk et al. [46,47] have reported that the presence of nitrogen in austenitic stainless steels strongly affects their electrochemical properties, which is a consequence of the electronic exchange between iron and nitrogen atoms in austenitic fcc lattice. Accordingly, the increase in free electron density—because of nitrogen atoms in iron lattice—favors the short range ordering and enhances the metallic character of interatomic bonds. Bonding between atoms of iron and nitrogen causes an enhanced thermodynamic stability and resistance against the corrosive environments.

3.2. Porosity evaluation

The porosity is an important index that determines the mechanical behavior of the alloy. The microstructural analysis investigated the presence of porosities. Fig. 9a, b and c indicate the SEM micrograph of the polished samples proceed via the BAE method containing 0, 3 and 6 wt% sintering aid, respectively, with all sintered at a temperature of 1150 °C. In the microstructure shown, the gray area indicates the austenite phase, while the dark regions represent the porosities.

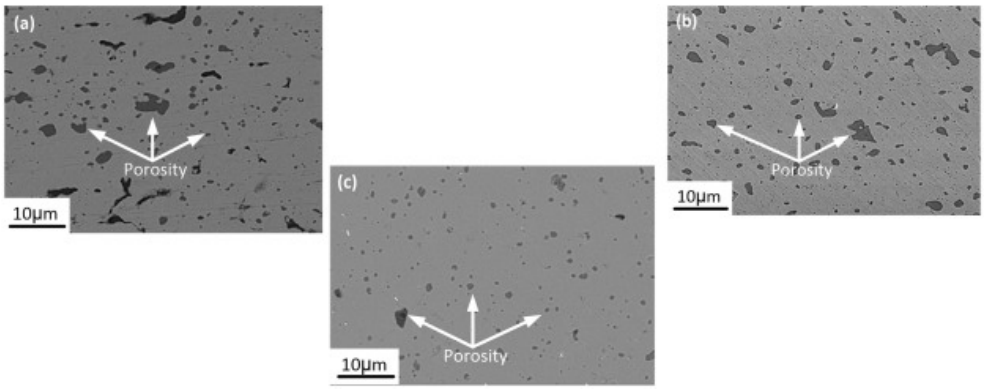

Fig. 9. SEM micrograph of polished samples containing (a) 0, (b) 3 and (c) 6 wt% sintering aid, all sintered at 1150 °C.

The microstructure of the polished sintered sample with 0 wt% sintering aid is shown in Fig. 9a. Coarse and multifaceted porosities are well visible in the image. Fig. 9b is the microstructure of the polished sintered sample with 3 wt% sintering aid. The micrograph signifies the contraction of the porosities caused by increasing the sintering aid content. Fig. 9c is the polished microstructure of the sintered sample containing 6 wt% sintering aid. The figure shows that the size and volume percentage of the pores have decreased considerably with the increase of the sintering aid to 6 wt%. The pictures also indicate that by increasing this additive, pore geometry tends to form a circular and round shape.

Image analyzer software was used to calculate the porosity percentages of the sintered samples. The results for three different samples are provided in Fig. 10. In the sample with 0 wt% sintering aid, the porosity is about 8.9%, while for 3 and 6 wt% sintering aid, the porosity percentages are about 8.5 and 6.8%, respectively. These results confirm that an increase in the sintering aid value leads to a considerable decrease in porosity percentage. The sintering aid (Mn-11.5 wt% Si) is an eutectic alloy with the melting point of 1140 °C [48]. Indeed, sintering at 1150 °C leads to melting of eutectic alloy and formation of a liquid phase in the components. The liquid phase penetrates due to capillarity force to pores, along with facilitated diffusivity and densification process [44]. This causes a noticeable decrease in size and also the shape of the porosities.

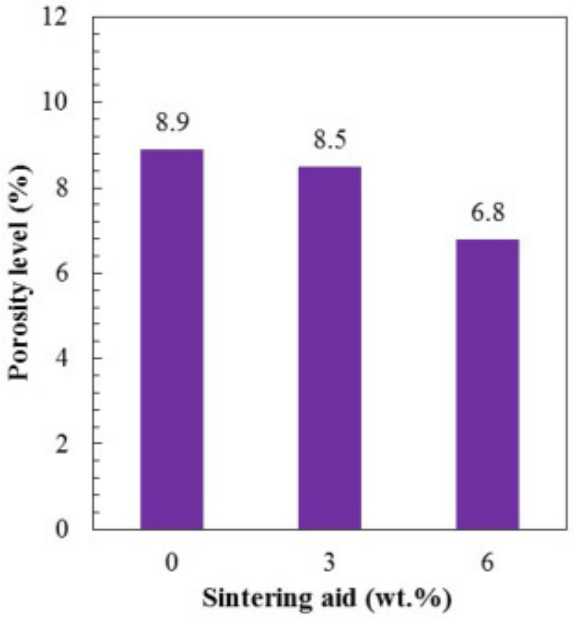

Fig. 10. Variation in porosities with sintering aid values.

These results indicate that the percentage of the porosities content for the sample with 6 wt% sintering aid fabricated by the BAE method is about 13.7% less than those samples that were produced by the PS method with the same values of sintering aid and sintering temperature, reported by Javanbakht and Salahinejad [35]. This decrease is related to the role of the binder in manufacturing processes. In the BAE process, the binder facilitates the better movement of the powder particles due to ball bearing action and improves filling the gaps between them [49,50]. Therefore, less porosity is retained between the particles during the paste preparation treatment.

3.3. Density evaluation

Densities of green samples have been obtained from measurements of the weight and volume of the specimens and using the equationρ=mv. The relative densities for samples with 0, 3 and 6 wt% sintering aid are measured as 5.7, 5.81 and 6.09 g/cm^3, respectively. The average green densities of the samples prepared by the PS method with 0, 3 and 6 wt% sintering aid is reported as 5.58, 5.75 and 5.83 g/cm^3, respectively [51]. The results indicate a 4% improvement in the green sample densities obtained by the BAE method with 6 wt% sintering aid.

The densities of the sintered samples were measured by the Archimedes method. The results for samples with 0, 3 and 6 wt% sintering aid are presented in Fig. 11. The results reveal that an increase of the sintering aid value from 0 to 6 wt% causes a 2.2% increase in the relative density of the sample. Comparison of the results obtained from the specimens fabricated by BAE and PS methods [51] show a 3% increase in the Archimedes density of the sample produced by the BAE method, with the same values of sintering aid and sintering temperature (6 wt% sintering aid and temperature of 1150 °C).

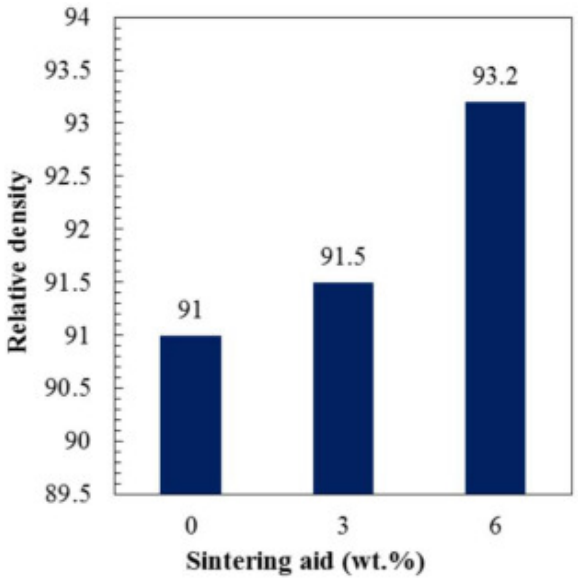

Fig. 11. Variation in densities of samples with sintering aid values.

3.4. Material characterization

The sample with 6 wt% sintering aid (Mn-11.5Si) was used to study material characterization. This sample had the least structural defects, so it was selected for study. The positive role of this sintering aid was approved elsewhere [35]. The elemental analysis of the final sintered sample was conducted by XRF and LECO. The chemical composition of the sample is Fe-16.1Cr-14.8Mn-2.9Mo-1Si-0.45 N-0.17C. It is noticeable that required chemical composition of ASTM F2581 has been obtained.

Fig. 12 shows the XRD analysis of the sintered samples containing 6 wt% sintering aid. The sharp observed peaks belong to iron (austenite phase). The small peaks between 30° and 45° and between 70°and 90° are related to chromium carbides and chromium nitrides. Due to the presence of carbon and nitrogen in the alloy, the formation of these compounds is inevitable. The x-ray diffraction pattern analysis was prepared by the Rietveld method. The results indicate that microstructure of the sample contains about 42% crystallite austenite phase, 55% amorphous phase and an insignificant amount of

the ferrites (about 0.01%). Ferrite phases cannot be detectable in the XRD pattern at such low levels. Ferrite is an undesirable phase in austenitic stainless steel medical grades, but its low values here can be ignored. The crystallite sizes determined by the XRD analysis are about 40 nm. It is well known that by developing a grain refining process, a significant improvement in mechanical properties —like strength, fracture and fatigue behavior— is attainable [10].

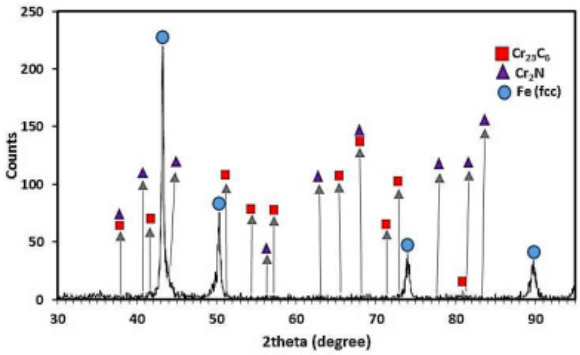

Fig. 12. XRD pattern of the sintered sample containing 6 wt% sintering aid.

Investigation of the microstructure by TEM is presented in Fig. 13. Two distinct areas can be seen in the microstructure. A relative shaded area and a white area are shown by A and B on the TEM images, respectively. Selected area diffraction (SAD) patterns are taken from the dark and white areas, as seen in Fig. 13. The SAD results indicate that the shaded area (A) is composed of a crystallite phase in the size of a few nanometers, while the white areas (B) are amorphous phases.

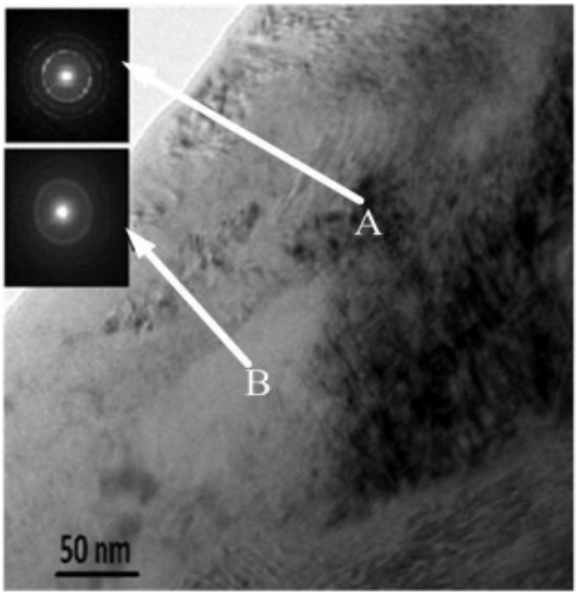

Fig. 13. TEM image of the sintered sample with 6 wt% sintering aid.

Mechanical alloying is a process that generates a high volume of dislocations in the microstructure. These dislocations have been arranged during sintering processes, producing subgrains and crystallite in nano-size. The method also causes amorphization in the microstructure. Amini et al. have proven the formation of these nanostructures and amorphization in the ball milling production processes of ASTM F2581 [52]. The nanostructure, formed during mechanical alloying, contains a high amount of

grain boundary areas per unit volume of the material. As a result of this structure, a considerable amount of energy is stored in the material as grain boundary energy. This energy provides a high driving force for grain growth at high temperatures when the atomic diffusion is fast enough.

The stability of the nanograins in such high temperatures (i.e., sintering temperature of 1150 °C) is an exciting subject. The reason why these nanosize grains are stable in such conditions may be attributed to the presence of excessive nitrogen in the structure [37,53]. The solubility of nitrogen inside the crystal is limited, thus tending to accumulate at the grain boundaries. The accumulation and segregation of this interstitial element at grain boundaries can prevent grain growth at high temperature [37]. Carbon can also play a similar role in the material [54]. Nitrogen and carbon, by a mechanism of locking mobile dislocation and fixing them, prevent the grain growth in the grain-refined structures. This was shown in our previous works [37,54]. Also, the Rietveld analysis has confirmed the formation of the amorphous phase in the microstructures. The previous study has also shown amorphization can be produced due to severe plastic deformation during mechanical alloying. In the amorphous areas, high-energy grain boundaries are not available. Therefore, the amorphous regions also avoid the grain growth phenomenon through the sintering processes.

It should be noted that the presence of nitrogen is also an essential factor in the stability of the amorphous phase and in retarding the nano-grain sizes. The encapsulation of the brown samples during sintering processes prevents excessive nitrogen from escaping the specimen (LECO's analysis indicates that only 0. 04% of the nitrogen was released) and maintains the stability of the amorphous phase and nano-size structure [11,37,51,55,56]. Similar behavior in structural refinement has been reported by the presence of boron in mechanically alloyed Co-based alloys [57].

The homogeneity of the alloy was investigated by taking the EDS-SEM map of Mn, Si and Cr (Fig. 14). Fig. 14a presents the SEM micrograph of a considered area, while Fig. 14b, c and d show a distribution of Mn, Si and Cr in the microstructure, respectively. The results reveal that the proper distribution of the alloying elements occurs in the microstructure of the samples processed by using the BAE method. Since the grains are nano-size and diffusion path is in the nanometer range, such homogeneity is provided [25].

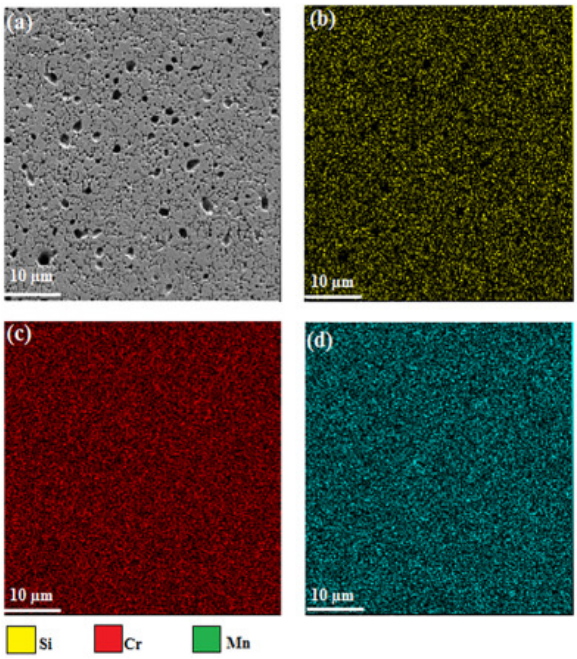

Fig. 14. (a) SEM micrograph and EDS map of (b) Mn, (c) Si and (d) Cr for the sintering aid-containing sample sintered at 1150 °C.

3.5. Mechanical properties analysis

The variation of hardness with increasing the sintering aid weight percentages is plotted in Fig. 15. The results show that the hardness of the samples with 0 wt% sintering aid is 295 HV, with 3 wt% sintering aid is 319 HV, and 6 wt% sintering aid is 339 HV. These results indicate that hardness of the samples increases by about 8% with adding 3 wt% sintering aid, and increased 13% with adding 6 wt% sintering aid. In comparison, the hardness of this steel is about two to three times higher than the hardness of a conventional AISI 316 L stainless steel, depending on the sintering aid values [7]. Hardness is the resistance of a material against plastic deformation, and plastic deformation is caused by the movement of dislocations [58]. The presence of very small grains with a high volume of grain boundaries in the microstructure generates local stress field that interacts with dislocations, impeding their motion and leading to an increase in the hardness properties of the material [59].

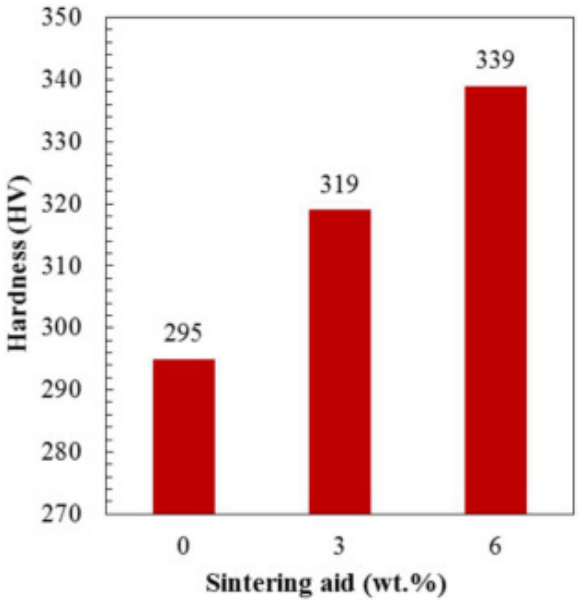

Fig. 15. The hardness values of samples with 0, 3 and 6 wt% sintering aid.

Fig. 16 shows the results of the stress-strain curve of the ASTM F2581 obtained by the BAE method and using varying amounts of sintering aid. These plots are derived from the compression tests on the samples with 0, 3 and 6 wt% of Mn-11.5 wt% Si sintering aid. In general, the slope of the stress-strain curve in the elastic area, which is defined as Young's modulus, increases by increasing the sintering aid weight percent. This implies a direct relationship between Young's modulus of the product samples and the increase in the sintering aid values. A power equation which properly explains this issue is:

(3)

$$E = E_0(1 - f_1\rho + f_2\rho^2)$$

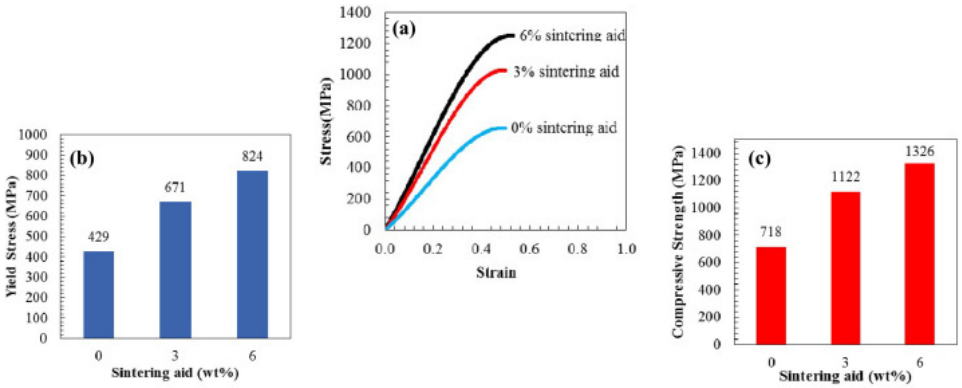

Fig. 16. (a) The true stress-strain curve, (b) yield strength and (c) compressive strength of the sintered samples at 1150 °C.

In which E is Young's modulus of porous samples, E_0 is Young's modulus of a dense sample, ρ is the porosity fraction, and f_1 and f_2 are constants of 1.9 and 0.9, respectively [37]. Young's modulus describes the elastic behavior of the alloy. One area of interest is the potential to modify the flexibility or bending stiffness of orthopedic implants through the use of engineering porosity [60]. For this issue, Young's modulus can be altered by variation in pore shape and distribution [60].

The stress-strain curve in Fig. 16a shows that departure from elastic to plastic state for ASTM F2581 has been progressed homogenously. This means that a distinctive yield point is not clear on the stress-strain plot. The yield strength was determined using a conventional offset method (offset 0.2%). Since the material did not fail during the compression test, the compressive strength was discovered at a strain of 50% for all states, according to ASTM E9 [61]. Fig. 16b and c indicate the variation of the yield and compressive strength of the samples with different values of the sintering aid. It is observed that the sample contains 0 wt% sintering aid and yields at a stress of 450 MPa. The compressive strength at this sintering aid percentage is 718 MPa. For the sample with 3 wt% sintering aid, the yield strength is obtained as 671 MPa and compressive strength is about 1122 MPa. The results indicate that by adding about 3 wt% of the sintering aid, an increase of 36% in the yield and compressive strength occurs. The increase is more noticeable as the sintering aid increases to 6 wt%. The samples obtained with this amount of sintering aid exhibit outstanding yield and compressive strength of 824 MPa and 1326 MPa, respectively. The values of the yield and compressive strength are about 48% and 46% larger than the sample with 0 wt% of the sintering aid.

As mentioned earlier, the alloy of ASTM F2581 was produced by Javanbakht et al. through the PS method using the same sintering aid and without using any binder [10,35]. The values of yield and compressive strength of the samples measured by the PS method are reported as 755 MPa and 1230 MPa, respectively [10]. Comparing the results obtained from the BAE and PS method shows 8.37% and 7.23% improvement in the yield and compressive strength, respectively, by using the BAE method. It is evident from the results that samples of ASTM F2581 obtained by BAE technique provide a considerable improvement in mechanical properties. The importance of manufacturing the ASTM F2581 austenitic stainless steel by the binder assisted extrusion method is more evident by comparing the mechanical properties of this steel with the austenitic stainless steel produced routinely by the hot rolling process. The yield and ultimate strength for the hot-rolled AISI 304 L stainless steel have been reported as 426 MPa and 673 MPa, respectively [62]. The results indicate that the yield and compression strength of ASTM F2581 obtained through the BAE method has increased by a factor of 2, as compared with the usual AISI 304 L stainless steel.

Ductility is another valuable mechanical property of metals for forming and shaping operations and for preventing catastrophic failure in services. In the compression test of ductile materials that does not fail during the test, the uniform elongation or strain of compressive strength may be a proper criterion to evaluate the ductility. In compression tests of samples with 0, 3 and 6 wt%, the sintering aid up to a 50% strain shows no brittle fracture, as shown in Fig. 17. This means that the alloy can practically undergo more than 50% deformation in pressure. The obtained ductility is comparable to dense-hot roll-steel and is much more than AISI 316LN steel [63].

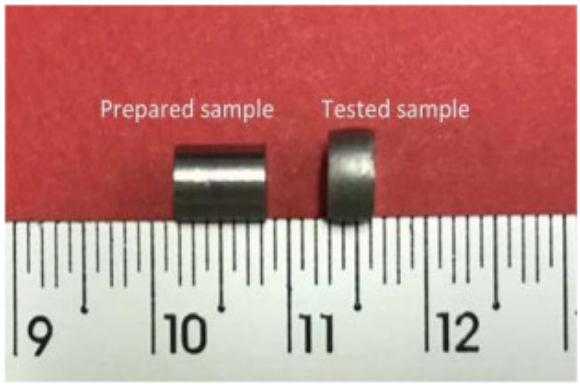

Fig. 17. Comparison of prepared compression test sample and tested sample according to ASTM E9 recommendations.

Achieving such respectable strength and ductility in nanocrystalline biomedical stainless steel grade is due to considering the new strategy in manufacturing processes. As mentioned earlier, a set of polymers was used in the powder preparation stage of the present study. Using the binder improved the fluidity of the powders and, therefore, considerably decreased the formation of the pores and large flaws in the microstructure. Another essential factor in the strength and ductility of the alloy are the shape and morphology of the pores. The rounded pores is less damaging than sharp, angular porosities [44]. The detrimental impact of sharp and angular pores is much more noticeable in terms of dynamic loading conditions than in static loading states. The sharp, angular porosity becomes a point of stress riser and a potential site for crack initiation and occurrence of a brittle fracture [44]. Changing the nature of pores from sharp and angular to a spherical shape and smaller size by using the binder aside sintering aid is seen in the microstructural analysis (Fig. 9).

Another noteworthy parameter in improving mechanical properties is the benefit of the grain refinement mechanism. The grain size of the ASTM F2581 alloy produced via the BAE method is in the range of the nano size and is much finer than the grain size of conventional commercial alloys, like AISI 304 L (about 20 µm from Fig. 4 of Ref. [62]. According to the Hall-Petch relation, the yield stress σ_y depends on the grain size *d* as [64].

(4)

$$\sigma_y = \sigma_0 + Kd^{-1/2}$$

where σ_0 is the friction stress, and *K* is a constant of the material.

Increasing the strength by decreasing the grain size is associated with the dislocation activity and the interaction with the grain boundaries obstacles. The dislocations sent out from dislocation sources, gliding on the slip plans and pile up at barriers such as grain boundaries [58]. The number of dislocations accumulating in piles is proportional to grain sizes. By decreasing the grain sizes, the number of dislocations in piles is reduced [58,64]. It is noteworthy that the leading dislocations in the pile up are forced not only by applying shear stress but also by the interaction of forces with the other dislocations accumulated in the pile up. The overcoming of the leading dislocation over grain boundary barriers and the occurring of plastic deformation require high-stress levels. In coarse-grain microstructures, some portion of the required forces is provided by a high volume of pile up

dislocations. In contrast, at a finer grain microstructure material, this source of forces is not available, and higher applied stress should act as the start of the plastic deformation or yielding.

Another mechanism that attributed to the improvement of the strength is the presence of supersaturated of nitrogen in the microstructure of the alloy [65,66]. The Fe_3N powders via mechanical alloying entered nitrogen into the microstructure [66]. The creation of the high density of defects along with the mechanical alloying significantly raises the nitrogen solubility, so a high concentration of the nitrogen entrapped at dislocation elastic stresses fields and causes them to be locked [66,67]. The immobility of dislocations due to interlocking with the nitrogen atoms through the microstructure [68,69] leads to a considerable increase in the strength.

It should be noted this ductility was measured under the compression test, and its value should be higher than those in tension test due to presence small amount of porosities in the microstructure. The failure of ductile metals in the tensile test consists of three-stages of void nucleation, growth and coalescence [70]. The presence of the porosities will reduce the ductility, since microvoids pre-exist before any stress is applied, and the nucleation stage of a ductile fracture is bypassed [71]. Moreover, porosity larger than a critical size in metals causes stress concentrations to occur near them. It results in local plastic deformation and the development of microcracks that decrease the metal tensile ductility [71]. Since the pores are closed in the compression test, they cannot cause the reduction of ductility in this state of loading.

3.1. Economic aspects

Since we proceed this alloy in our laboratory by both BAE and hot powder forge [36], cost analysis was performed for these two methods. An approximate cost of making a sample is 265 € per kilogram which includes the cost of raw materials, additive cost, and extrusion cost for sintering operation. To produce one kilogram part by hot powder forging method, there is a need to use hot forge at a cost of 110 € per hour. If we consider a five-hour time to produce parts in hot powder forge, we can estimate that 2 times of the total cost can be saved in production of nickel free stainless steel using BAE method compare with the hot powder forge technique. It should be noted that the price calculation here is for the laboratory scale and at the industrial scale the prices are much lower.

4. Conclusion

ASTM F2581 nanostructured nickel-free stainless steel for medical applications was fabricated by using the BAE method alongside 0, 3 and 6 wt% sintering aid. It has been determined that the binder has a significant effect on the paste characteristics and the sintering processes. The prepared specimens with optimal contents of binder show the formation of nanostructure and a considerable decrease of the pores, leading to high densities and outstanding improvements of the mechanical properties, such as hardness and compressive strength. For the optimum specimen, the results indicate yield strength up to 824 MPa, compressive strength up to 1326 MPa, uniform elongation in the range of 50% and hardness properties of 339 HV. The method is utilized for the first time for making medical-grade stainless steel. It facilitates the production of large-size components, which are usually too difficult to make using other powder metallurgy techniques.

Declaration of Competing Interest

The authors declare that they have no known competing financial interests or personal relationships that could have appeared to influence the work reported in this paper.

Acknowledgments

The authors would like to acknowledge the Material Science and Engineering Laboratory of the Shiraz University in fulfillment of this investigation.

References

[1] P. Mahmoudi Hashemi, E. Borhani, M.S. Nourbakhsh. **A review on nanostructured stainless steel implants for biomedical application.** Nanomed. J., 3 (2016), pp. 202-216

[2] J. Disegi, L. Eschbach. **Stainless steel in bone surgery.** Injury, 31 (2000), pp. D2-D6

[3] Q. Chen, G.A. Thouas. **Metallic implant biomaterials.** Mater. Sci. Eng. R. Rep., 87 (2015), pp. 1-57

[4] S.H. Teoh. **Engineering materials for biomedical applications.** World Scientific (2004)

[5] M. Niinomi, M. Nakai, J. Hieda. **Development of new metallic alloys for biomedical applications.** Acta Biomater., 8 (2012), pp. 3888-3903

[6] M. Talha, C. Behera, O. Sinha. **A review on nickel-free nitrogen containing austenitic stainless steels for biomedical applications.** Mater. Sci. Eng. C, 33 (2013), pp. 3563-3575

[7] K. Yang, Y. Ren. **Nickel-free austenitic stainless steels for medical applications.** Sci. Technol. Adv. Mater., 11 (2010), p. 014105

[8] M. Sumita, T. Hanawa, S. Teoh. **Development of nitrogen-containing nickel-free austenitic stainless steels for metallic biomaterials.** Mater. Sci. Eng. C, 24 (2004), pp. 753-760

[9] M. Talha, C. Behera, O. Sinha. **Effect of nitrogen and cold working on structural and mechanical behavior of Ni-free nitrogen containing austenitic stainless steels for biomedical applications.** Mater. Sci. Eng. C, 47 (2015), pp. 196-203

[10] M. Javanbakht, E. Salahinejad, M. Hadianfard. **The effect of sintering temperature on the structure and mechanical properties of medical-grade powder metallurgy stainless steels.** Powder Technol., 289 (2016), pp. 37-43

[11] C. Suryanarayana. **Mechanical alloying and milling.** Prog. Mater. Sci., 46 (2001), pp. 1-184

[12] C.C. Koch. **Structural nanocrystalline materials: an overview.** J. Mater. Sci., 42 (2007), pp. 1403-1414

[13] R. Scattergood, C. Koch, K. Murty, D. Brenner. **Strengthening mechanisms in nanocrystalline alloys.** Mater. Sci. Eng. A, 493 (2008), pp. 3-11

[14] W. Mook, M. Lund, C. Leighton, W. Gerberich. **Flow stresses and activation volumes for highly deformed nanoposts.** Mater. Sci. Eng. A, 493 (2008), pp. 12-20

[15] H. Ueno, K. Kakihata, Y. Kaneko, S. Hashimoto, A. Vinogradov. **Enhanced fatigue properties of nanostructured austenitic SUS 316L stainless steel.** Acta Mater., 59 (2011), pp. 7060-7069

[16] I. Ovid'Ko, R. Valiev, Y. Zhu. **Review on superior strength and enhanced ductility of metallic nanomaterials.** Prog. Mater. Sci., 94 (2018), pp. 462-540

[17] D. Farkas, S. Mohanty, J. Monk. **Strain-driven grain boundary motion in nanocrystalline materials.** Mater. Sci. Eng. A, 493 (2008), pp. 33-40

[18] D. Wu, J. Zhang, J. Huang, H. Bei, T.-G. Nieh. **Grain-boundary strengthening in nanocrystalline chromium and the hall–Petch coefficient of body-centered cubic metals.** Scr. Mater., 68 (2013), pp. 118-121

[19] A. Khalifeh, A.D. Banaraki, H.D. Manesh, M.D. Banaraki. **Investigating of the tensile mechanical properties of structural steels at high strain rates.** Mater. Sci. Eng. A, 712 (2018), pp. 232-239
[20] E. Aifantis. **Deformation and failure of bulk nanograined and ultrafine-grained materials.** Mater. Sci. Eng. A, 503 (2009), pp. 190-197
[21] B. Al-Mangour. **Powder metallurgy of stainless steel: state-of-the art, challenges, and development.** Stainless Steel: Microstructure, Mechanical Properties and Methods of Application, 80, Nova Science Publishers (2015), p. 37
[22] M. Aslam, F. Ahmad, P.S.M.B.M. Yusoff, K. Altaf, M.A. Omar, R.M. German. **Powder injection molding of biocompatible stainless steel biodevices.** Powder Technol., 295 (2016), pp. 84-95
[23] M.R. Raza, F. Ahmad, N. Muhamad, A.B. Sulong, M. Omar, M.N. Akhtar, M. Aslam. **Effects of solid loading and cooling rate on the mechanical properties and corrosion behavior of powder injection molded 316 L stainless steel.** Powder Technol., 289 (2016), pp. 135-142
[24] P. Angelo, R. Subramanian. **Powder Metallurgy: Science, Technology and Applications.** PHI Learning Pvt. Ltd (2008)
[25] E. Salahinejad, M.J. Hadianfard, M. Ghaffari, S.B. Mashhadi, A.K. Okyay. **Fabrication of nanostructured medical-grade stainless steel by mechanical alloying and subsequent liquid-phase sintering.** Metall. Mater. Trans. A, 43 (2012), pp. 2994-2998
[26] Z. Chen, K. Ikeda, T. Murakami, T. Takeda. **Drainage phenomenon of pastes during extrusion.** J. Mater. Sci., 35 (2000), pp. 2517-2523
[27] F. Händle. **Extrusion in Ceramics: Engineering Materials and Processes.** Springer (2007)
[28] J. Benbow, J. Bridgwater. **Paste flow and extrusion.** (1993)
[29] J. Benbow, J. Bridgwater. **The influence of formulation on extrudate structure and strength.** Chem. Eng. Sci., 42 (1987), pp. 753-766
[30] J. Benbow, S. Jazayeri, J. Bridgwater. **The flow of pastes through dies of complicated geometry.** Powder Technol., 65 (1991), pp. 393-401
[31] J.A. Mangels, G.L. Messing. **Advances in Ceramics: Vol. IX, Forming of Ceramics.** (1984)
[32] H. TAKEBE, M. YOSHIDA, K. HAYASHI, K. MORINAGA. **Fabrication of alumina sheets by extrusion.** J. Ceram. Soc. Jpn., 100 (1992), pp. 750-754
[33] H. Böhm, S. Blackburn. **Agglomerate breakdown in fine alumina powder by multiple extrusion.** J. Mater. Sci., 29 (1994), pp. 5779-5786
[34] E. Salahinejad, M.J. Hadianfard, D.D. Macdonald, S. Sharifi-Asl, M. Mozafari, K.J. Walker, A.T. Rad, S.V. Madihally, L. Tayebi. **In vitro electrochemical corrosion and cell viability studies on nickel-free stainless steel orthopedic implants.** PLoS One, 8 (2013)
[35] M. Javanbakht, M. Hadianfard, E. Salahinejad. **Microstructure and mechanical properties of a new group of nanocrystalline medical-grade stainless steels prepared by powder metallurgy.** J. Alloys Compd., 624 (2015), pp. 17-21
[36] L. Heidari, A. Tangestani, M. Hadianfard, D. Vashaee, L. Tayebi. **Effect of fabrication method on the structure and properties of a nanostructured nickel-free stainless steel.** Adv. Powder Technol., 31 (2020), pp. 3408-3419
[37] E. Salahinejad, R. Amini, M. Hadianfard. **Contribution of nitrogen concentration to compressive elastic modulus of 18Cr–12Mn–xN austenitic stainless steels developed by powder metallurgy.** Mater. Des., 31 (2010), pp. 2241-2244
[38] A. Standard. **E9-09, Standard test methods of compression testing of metallic materials at room temperature.** (2009)

[39] R. German. **Powder injection molding applications to new materials.** 680, BOOK-INSTITUTE OF MATERIALS (1998), pp. 1363-1376
[40] W. Loue, M. Suery, J. Querbes. **Microstructure and rheology of partially remelted AlSi-alloys.** Proc. 2nd Int. Conf. on the Semi-Solid Processing of Alloys and Composites, Cambridge, Massachussets (1992), pp. 266-275
[41] X. Lu, Y. Lee, S. Yang, Y. Hao, J.R. Evans, C.G. Parini. **Solvent-based paste extrusion solid freeforming.** J. Eur. Ceram. Soc., 30 (2010), pp. 1-10
[42] M. Rahaman. **Ceramic Processing and Sintering.** 264, Marcel Dekker, Inc., New York (1995)
[43] N. Vitorino, C. Freitas, M. Ribeiro, J. Abrantes, J. Frade. **Extrusion of ceramic emulsions: plastic behavior.** Appl. Clay Sci., 101 (2014), pp. 315-319
[44] E. Klar, P.K. Samal. **Powder metallurgy stainless steels: processing, microstructures, and properties.** ASM Int., 59-100 (2007)
[45] M. Metikoš-Huković, R. Babić, Z. Grubač, Ž. Petrović, N. Lajçi. **High corrosion resistance of austenitic stainless steel alloyed with nitrogen in an acid solution.** Corros. Sci., 53 (2011), pp. 2176-2183
[46] V. Gavriljuk, B. Shanina, H. Berns. **A physical concept for alloying steels with carbon+ nitrogen.** Mater. Sci. Eng. A, 481 (2008), pp. 707-712
[47] V. Gavriljuk, B. Shanina, H. Berns. **On the correlation between electron structure and short range atomic order in iron-based alloys.** Acta Mater., 48 (2000), pp. 3879-3893
[48] H. Baker, H. Okamoto. **ASM Handbook.** Alloy Phase Diagrams, ASM International, Materials Park, Ohio 44073–0002, USA, Vol. 3 (1992) 1992. 501
[49] P.K. Johnson. **Iron Powder Metallurgy.** Springer (2013)
[50] K. Yousefi, H.D. Manesh, A. Khalifeh, F. Moazami, M. Sanaee. **Nanocement/poly (vinyl alcohol) composites for endodontic applications.** Mater. Chem. Phys., 123337 (2020)
[51] E. Salahinejad, M. Hadianfard, M. Ghaffari, S.B. Mashhadi, A. Okyay. **Liquid-phase sintering of medical-grade P558 stainless steel using a new biocompatible eutectic additive.** Mater. Lett., 74 (2012), pp. 209-212
[52] E. Salahinejad, M. Hadianfard, M. Ghaffari, R. Amini, S.B. Mashhadi, A. Okyay. **Microstructural characterization of medical-grade stainless steel powders prepared by mechanical alloying and subsequent annealing.** Adv. Powder Technol., 24 (2013), pp. 605-608
[53] E. Salahinejad, R. Amini, M. Hadianfard. **Structural evolution during mechanical alloying of stainless steels under nitrogen.** Powder Technol., 215 (2012), pp. 247-253
[54] E. Salahinejad, R. Amini, M. Marasi, M. Hadianfard. **Microstructure and wear behavior of a porous nanocrystalline nickel-free austenitic stainless steel developed by powder metallurgy.** Mater. Des., 31 (2010), pp. 2259-2263
[55] E. Salahinejad, R. Amini, M. Hadianfard. **Effect of milling time on structure and mechanical properties of porous nickel-free austenitic stainless steels processed by mechanical alloying and sintering.** Mater. Sci. Eng. A, 527 (2010), pp. 5522-5527
[56] R. Amini, M. Hadianfard, E. Salahinejad, M. Marasi, T. Sritharan. **Microstructural phase evaluation of high-nitrogen Fe–Cr–Mn alloy powders synthesized by the mechanical alloying process.** J. Mater. Sci., 44 (2009), p. 136
[57] A.H. Taghvaei, M. Stoica, G. Vaughan, M. Ghaffari, S. Maleksaeedi, K. Janghorban. **Microstructural characterization and amorphous phase formation in Co40Fe22Ta8B30 powders produced by mechanical alloying.** J. Alloys Compd., 512 (2012), pp. 85-93
[58] G.E. Dieter, D.J. Bacon. **Mechanical Metallurgy.** McGraw-hill New York (1986)

[59] M. Dewald, W. Curtin. **Multiscale modelling of dislocation/grain boundary interactions. II. Screw dislocations impinging on tilt boundaries in Al.** Philos. Mag., 87 (2007), pp. 4615-4641
[60] J.A. Choren, S.M. Heinrich, M.B. Silver-Thorn. **Young's modulus and volume porosity relationships for additive manufacturing applications.** J. Mater. Sci., 48 (2013), pp. 5103-5112
[61] E. ASTM. **Standard test methods of compression testing of metallic materials at room temperature, west Conshohocken, PA.** ASTM Int. (2000), pp. 98-105
[62] A. Khalifeh, A. Dehghan, E. Hajjari. **Dissimilar joining of AISI 304L/St37 steels by TIG welding process.** Acta Metallurgica Sinica (English Letters), 26 (2013), pp. 721-727
[63] B.S. Dutt, G. Shanthi, G. Sasikala, M.N. Babu, S. Venugopal, S.K. Albert, A. Bhaduri, T. Jayakumar. **Effect of nitrogen addition and test temperatures on elastic-plastic fracture toughness of SS 316 LN.** Procedia Eng., 86 (2014), pp. 302-307
[64] Y. Estrin, A. Vinogradov. **Extreme grain refinement by severe plastic deformation: a wealth of challenging science.** Acta Mater., 61 (2013), pp. 782-817
[65] C. Garcia-Cabezon, Y. Blanco, M.L. Rodriguez-Mendez, F. Martin-Pedrosa. **Characterization of porous nickel-free austenitic stainless steel prepared by mechanical alloying.** J. Alloys Compd., 716 (2017), pp. 46-55
[66] E. Salahinejad, R. Amini, M. Ghaffari, M. Hadianfard. **Crystal interstitial sites contribution to nitrogen supersaturation in mechanically alloyed Fe–Cr–Mn–N alloys.** J. Alloys Compd., 505 (2010), pp. 584-587
[67] M. Byrnes, M. Grujicic, W. Owen. **Nitrogen strengthening of a stable austenitic stainless steel.** Acta Metall., 35 (1987), pp. 1853-1862
[68] A.-C. 318. **Building Code Requirements for Structural Concrete and Commentary (ACI 318–08).** American Concrete Institute Farmington Hills^ eMI MI (2011)
[69] S. Lou, D. Northwood. **Effect of temperature on the lower yield strength and static strain ageing in low-carbon steels.** J. Mater. Sci., 30 (1995), pp. 1434-1438
[70] T.L. Anderson, T.L. Anderson. **Fracture Mechanics: Fundamentals and Applications.** CRC press (2005)
[71] R. Hardin, C. Beckermann. **Effect of porosity on deformation, damage, and fracture of cast steel.** Metall. Mater. Trans. A, 44 (2013), pp. 5316-5332